EARTHQUAKE ENGINEERING AND STRUCTURAL DYNAMICS
Earthquake Engng Struct. Dyn. 2009; **38**:759–781
Published online 17 November 2008 in Wiley InterScience (www.interscience.wiley.com). DOI: 10.1002/eqe.865

Seismic performance evaluation of a 34-story steel building retrofitted with response modification elements

Yuan-Tao Weng[1,‡], Keh-Chyuan Tsai[2,*,†,§,¶], Pei-Ching Chen[2,‖], Chung-Che Chou[2,**], Ya-Ran Chan[2,‖], Sheng-Jhih Jhuang[1,††] and Yung-Yu Wang[3,‖]

[1]*National Center for Research on Earthquake Engineering, Taipei, Taiwan*
[2]*National Taiwan University, Taipei, Taiwan*
[3]*Tongji University, Shanghai 200092, China*

SUMMARY

The original structural design of this case study consisted of five basement floors and a 34-story hotel tower in Kaohsiung, Taiwan. The construction started in 1993, and the erection of the entire steel frame and the pouring of concrete slabs up to the 26th floor were completed before 1996. However, construction of the original hotel was subsequently suspended for 10 years. Recently, this building has been retrofitted for residential purposes. Buckling restrained braces (BRBs) and eccentrically braced frames were incorporated into the seismic design of the new residential tower. This paper presents the seismic resisting structural system, seismic design criteria, full-scale test results of one BRB member and the as-built welded moment connections. Test results confirm that the two side web-plate stiffening details can effectively improve the rotational capacity of welded moment connection. The paper also discusses the analytical models for simulating the experimental responses of the BRB members and the welded moment connections. Nonlinear response history analyses (NLRHA) indicate that the inelastic deformational demands of the original and the redesigned structures induced by the maximum considered earthquakes are less than those found in the seismic building codes or laboratory tests. This paper also proposes a ground motion scaling method considering multi-mode effects for NLRHA of the example building. It is shown that the proposed scaling method worked well in reducing the scatter in estimated peak seismic demands. Copyright © 2008 John Wiley & Sons, Ltd.

Received 15 January 2008; Revised 8 September 2008; Accepted 10 September 2008

KEY WORDS: seismic retrofit; BRB; EBF; welded moment connection; nonlinear analysis; ground motion scaling method

*Correspondence to: Keh-Chyuan Tsai, National Taiwan University, Taipei, Taiwan.
†E-mail: kctsai@ncree.org.tw
‡Associate Research Fellow.
§Professor of Civil Engineering.
¶Director of National Center for Research on Earthquake Engineering.
‖Graduate Student.
**Associate Professor of Civil Engineering.
††Assistant Research Fellow.

1. INTRODUCTION

The original structural design was for a hotel tower in Kaohsiung, Taiwan. It is a steel frame building, which consists of five basement floors and a 34-story tower. Construction of the tower started in 1993, and the erection of the entire steel structure and the pouring of concrete slabs up to the 26th floor were completed before 1996. Owing to financial difficulties faced by the developer, the construction of the original hotel was suspended for 10 years. Recently, this building has been retrofitted and remodeled for residential purposes. The building height remains almost the same, but the floor area in some of the lower floors is reduced, whereas vice versa for the higher floors. The original structural system was no longer able to meet the new seismic force requirements mandated in 2005. In order to meet the more stringent seismic performance requirements, buckling restrained brace (BRB) members and new eccentrically braced frame (EBF) configurations were incorporated into the seismic design of the new residential tower. To verify the rotational capacity of the existing welded moment connections, two as-built welded beam–column moment connections were removed from the construction site. A novel stiffening scheme was developed and applied in strengthening one of the connections before tests were carried out to compare the performance of the existing and the stiffened connection details. In this paper, the change of seismic force requirements is presented, and the new seismic performance requirements for this building are discussed. In addition, test results are presented and analytical models for simulating the experimental responses of the BRB and the stiffened welded moment connection were examined. Finally, the seismic performance of the structural system and response modification elements was evaluated by conducting 3-D NLRHA of the original and redesigned structures subjected to design-based earthquakes in two principal axis.

When nonlinear dynamic time-history analyses are conducted as part of a performance-based seismic design approach, the analyses often require the ground motion records be scaled to a specified level of seismic intensity. The elastic dynamic analysis procedures in the current Taiwan seismic design provisions [1] prescribe that a series of time-history analyses are required with ground motion records selected from no less than three events. After scaling the dynamic base shear

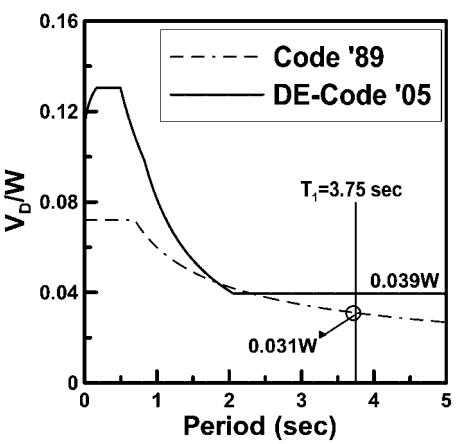

Figure 1. Design force/structural weight spectra.

DOI: 10.1002/eqe

with respect to the static design base shear, the maximum values of all the response parameters, such as inter-story drift or member forces, were adopted in the design. However, research shows that some scaling methods could introduce a very large scatter in the analysis results [2–5]. If the design response spectrum represents the design target that the structural engineer aims to achieve, then the large scatter resulted from a specific scaling method suggests that the seismic demand estimates may be biased. It could lead to designs with significant uncertainties and unknown safety margins, unless the average of a relatively large number of records is used [2]. In addition, for high-rise buildings, multi-mode effects are not adequately considered in some common ground motion scaling methods. This paper investigate a multi-mode ground motion scaling (MMS) method and applied it herein to the 34-story steel building. Especially, this method takes into account the modal characteristics and minimizes the difference between the spectral responses of a given ground motion and the smoothed design response spectrum at the first few modes.

2. BUILDING STRUCTURE DESIGN

2.1. Original structural system

The original hotel tower was designed and built as a dual system consisting of steel EBFs and special moment resisting frames using the Taiwan 1989 Code provisions for seismic force requirements (Code'89) [6]. The 1989 and 2005 versions of design force requirements are shown in Figure 1 in terms of the weight of the structure. The structural framing plan of the original hotel tower is similar to those shown in Figure 2. The floor construction consists of 15 cm thick concrete slab with metal deck over steel framing. The design live load (LL) for the hotel room was $2.0\,\mathrm{kN/m^2}$. The total height of the original hotel building was 124.7 m. The occupancy importance factor I was 1.25. All columns are of built-up box shape using A572 Grade 50 steel, whereas the rolled wide flange beams are mostly A36. The hotel building fundamental periods computed using the analytical model were 4.27 and 3.74 s in the longitudinal and transverse directions, respectively. The design seismic base shears based on the Code '89 were 0.033 W (based on $I=1.25$) for both directions, as the vibration period was governed by the empirical formula, $T_{\max}=1.4(0.07\,\mathrm{h}^{3/4})=3.66\,\mathrm{s}$.

2.2. Redesigned structural system

2.2.1. Design loads. The building has then been retrofitted and remodeled since 2006. The building height remains almost the same, but the floor area in some of the lower floors is reduced, whereas vice versa for the higher floors. Although the total height has been increased slightly from 124.7 to 128 m, substantial weight of the building has been shifted from the lower floors to the higher floors due to the new architectural configuration. The average floor dead load (DL) including all the walls is about $7.0\,\mathrm{kN/m^2}$, and the design LL for the residential unit is $2.0\,\mathrm{kN/m^2}$. Compared with Code'89, the 2005 version of seismic force requirements (Code'05) for buildings has changed rather significantly (refer to Figure 1). However, before retrofitting, this building has already got the building permit. Therefore, the Kaohsiung City Building Department treated this project as an unfinished case. The Kaohsiung City Building Department and the structural design review committee agreed with the structural engineers to maintain the use of the same response spectrum suggested in Code '89 for the building seismic retrofit and reconstruction for residential purposes. Nevertheless, the occupancy importance factor I was allowed to change from 1.25 for a major hotel to 1.0 for a residential building. Using the LRFD approach, design load combinations

DOI: 10.1002/eqe

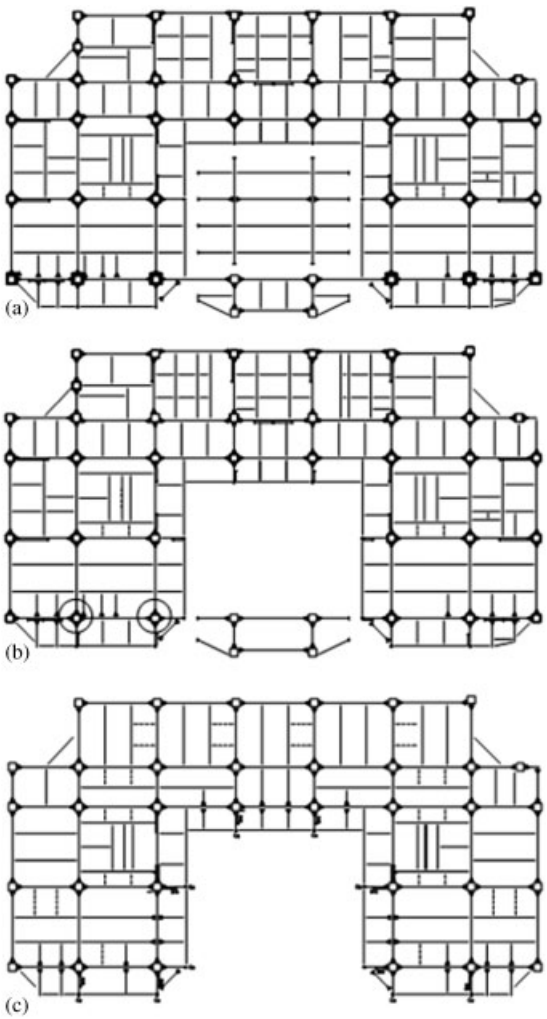

Figure 2. Typical floor framing plan of the building: (a) 1st to 11th stories; (b) 12th to 25th stories; and (c) 26th to 34th stories.

include: (1) 1.4DL, (2) 1.2DL+1.6LL, (3) 1.2DL+0.5LL+1.6WL, (4) 1.2DL+0.5LL+1.0EQ, (5) 0.9DL–1.0EQ and (6) 0.9DL–1.6WL. The redesigned building fundamental periods computed using the analytical model are 3.75 and 3.59 s in the longitudinal and transverse directions, respectively. Thus, the design base shear was reduced from 0.033 W for the original hotel building to 0.031 W (14 276 kN) computed based on the empirical vibration period of 3.75 s for the two principal building axis. The design base shear would have to be increased by 26% from 0.033 (for the original hotel building) to 0.039 W if the Code'05 was to be followed (Figure 1). Thus, the design engineers agreed to conduct detailed NLRHA using synthetic ground acceleration compatible with the elastic response spectrum prescribed in Code'05 [1]. The NLRHA and the performance of the redesigned super structure will be presented in detail later in this paper.

DOI: 10.1002/eqe

2.2.2. Upgrading of seismic force resisting system. Considering some structural members had deteriorated much due to weathering after construction was suspended for many years, it was decided that all steel framing above the 26th floor be removed. New EBFs were chosen for strengthening the 12 to 25th stories whenever the structural and architectural designs allow the installation of the new brace but require accommodating a door opening. In order to enhance the seismic performance of this building, A572 Grade 50 steel BRB elements were added into 1 to 11th stories whenever there was no requirements of providing door opening. All the new or existing link beams in the EBFs are shear links with a length smaller than $1.1M_p/V_p$, where M_p and V_p are beam plastic moment and shear capacities, respectively. Since the pouring of concrete slabs up to the 26th floor was completed before the re-construction, all the existing frame girders using the pre-Northridge type of welded moment connections could not be conveniently removed below the 26th floor. Thus, a new beam-to-column connection stiffening scheme using two steel web side plates was proposed. The side plates can be conveniently installed in the welded moment connections without removing the concrete slab above the beam flange. It was tested before implementing it into strengthening all the existing welded moment connections. Figures 2 and 3 display the typical floor framing plans and the elevations of this redesigned building. The specimen design and the test results are presented in this paper.

3. CYCLIC TESTS FOR AS-BUILT WELDED BEAM–COLUMN MOMENT CONNECTIONS

The proposed stiffening scheme was applied to the beam-to-column moment connections to ensure that the rotational capacity of welded moment connections is sufficient to meet the latest modern seismic steel building design provisions. To verify the feasibility of the stiffening scheme for the beam–column connections, two as-built welded beam–column moment connection subassemblies were cut from the 33th floor. These two specimens are designated as Specimens 1 and 2, which represent the steel beam without and with the proposed stiffening scheme, respectively. ASTM A36 and Grade 50 materials were specified for the beam and tube column, respectively. Specimen 1 includes one steel roll-shaped beam ($H702 \times 254 \times 16 \times 28$ mm) and one built-up box column ($700 \times 700 \times 35$ mm). On the other hand, Specimen 2 includes one steel roll-shaped beam ($H688 \times 255 \times 13 \times 21$) and a box column ($700 \times 696 \times 35$). The material properties of the beam specimens are included in Table I. The stiffeners were proportioned so that when the plastic hinge forms and strain hardens to 1.25 times the flexural capacity of the bare steel beam section at the stiffener edge, the flexural demand on the column face is no greater than 80% of the flexural capacity of the stiffened beam section. Figure 4(a) shows the details of the proposed strengthening scheme: two 20 mm thick full height steel and 300 mm length web side plates were welded to the column face and to the edges of the top and bottom flanges of the beam end. Experimental setup is shown in Figure 4(b) and the cyclic loads were applied horizontally at the cantilever beam end. Figure 4(c) shows the typical beam-to-column connections retrofitted at the site using the proposed web side plate details.

3.1. Test results

Based on the loading protocol described in the seismic provisions for steel building [7], Figures 5(a) and (c) show the rotational capacity of the Specimen 1 and the Specimen 2 are 3.0 and 4.0% rad, respectively. Figure 5(a) shows the beam force versus deformation relationships for Specimen 1.

DOI: 10.1002/eqe

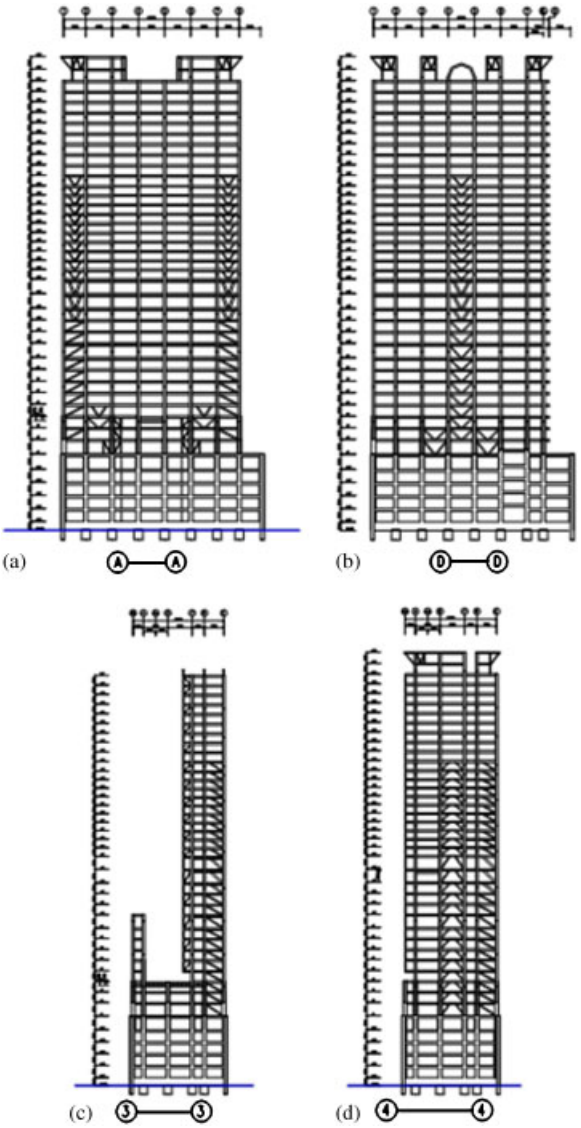

Figure 3. Elevations of the building: (a) Frame A; (b) Frame D; (c) Frame 3; and (d) Frame 4.

The beam top and bottom flanges yielded when the beam end rotation reached 0.01 and 0.015 rad, respectively. The maximum moment of Specimen 1 was 1.35 times the plastic moment capacity ($1.35M_{np}$ or 2576 kN-m) when the beam end rotation reached 0.03 rad. Before the beam reached 0.04 rad for the total rotation, the top flange fractured starting from the edge of the flange weld (Figure 5(b)). The cantilever beam load dropped to about 50% of the peak load. On the other hand, Figure 5(c) illustrates the beam force versus deformation relationships for Specimen 2. The maximum beam moment of Specimen 2 was $1.5\,M_{np}$ (1865 kN-m) when beam end rotation reached

DOI: 10.1002/eqe

Table I. Specimen member sizes and material properties.

	Member sizes		Beam material properties		
Specimen no.	Columns	Beams	Location	Yielding strength (MPa)	Ultimate strength (MPa)
1	$700\times700\times35\times35$	$H702\times254\times16\times28$ (W27×146)	Flange	275	485
			Web	288	495
2	$700\times696\times35\times35$	$H688\times255\times13\times21$ (W27×102)	Flange	250	418
			Web	385	437

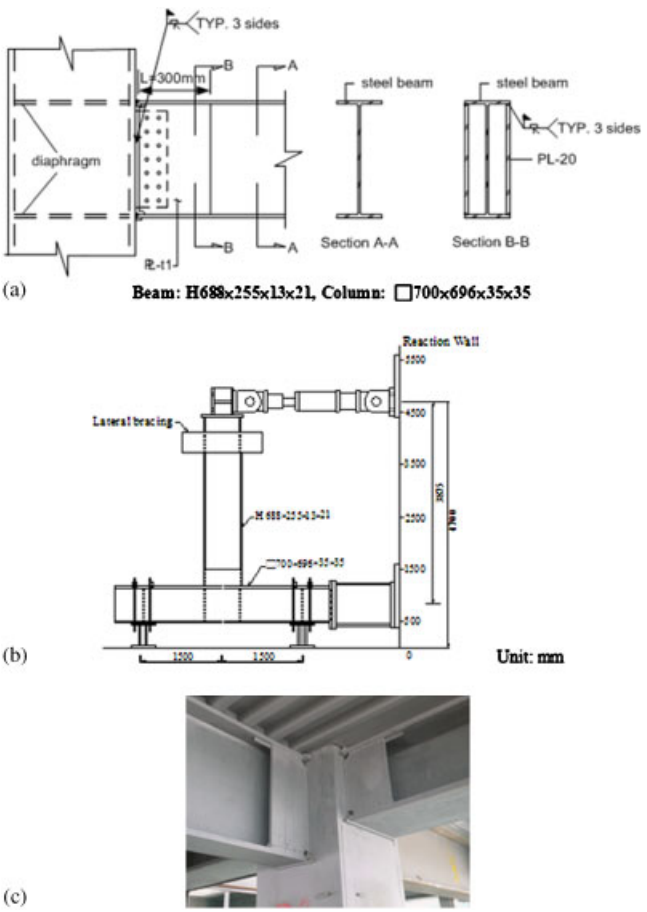

Figure 4. (a) The strengthening details of the welded moment connections; (b) setup of cyclic loading test; and (c) a photo of the two steel web side plate stiffening details.

0.03 rad. After reaching the peak load, the beam strength started to decrease as local buckling occurred at the beam flange when cyclic deformation increased. The beam load dropped 38% from the peak load when the beam end rotation reached 4.7% rad. However, no crack of base metal or

DOI: 10.1002/eqe

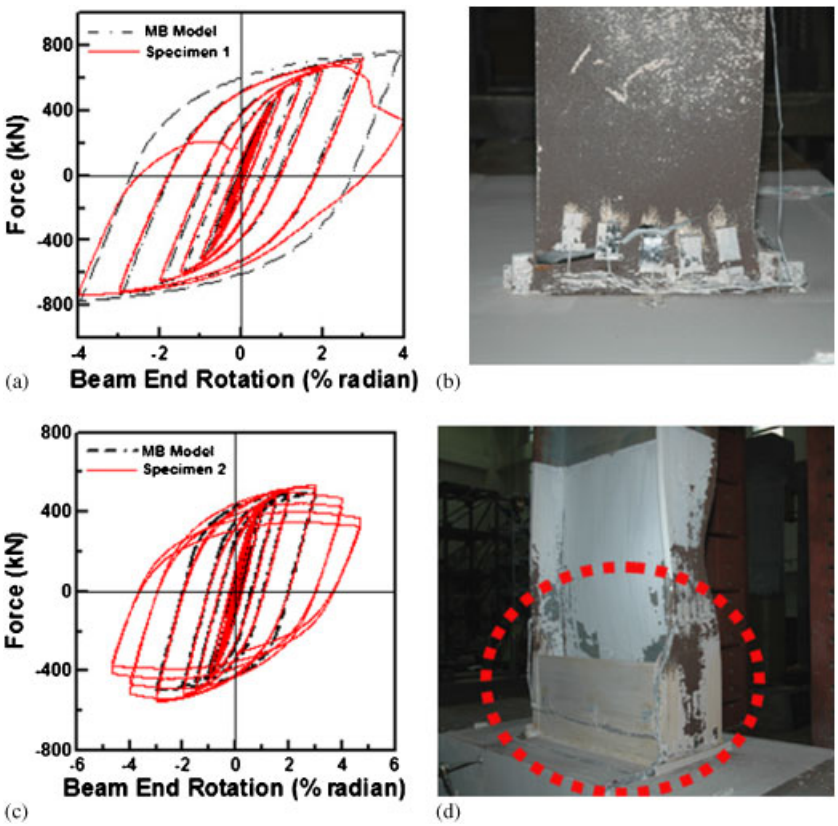

Figure 5. Cyclic test results: (a) beam force versus deformation relationships for Specimen 1; (b) flange buckling and cracking in Specimen 1; (c) beam force versus deformation relationships for Specimen 2; and (d) flange buckling in Specimen 2.

weld was observed (Figure 5(d)). The maximum flexural strains measured at the beam flanges near the column face are shown in Figure 6. It is evident that the proposed stiffening scheme effectively reduces the maximum strain of the beam flange.

4. ANALYTICAL MODEL

4.1. Introduction of PISA3D

The platform of inelastic structural analysis for 3D systems (PISA3D), developed in NTU and NCREE [8], is an object-oriented general-purpose computational platform for nonlinear structural analysis. It provides more than 35 different characteristics of structural elements for simulation of structural responses. In particular, its beam–column element can conveniently simulate the shear yielding or flexural yielding responses of steel wide flange sections. Thus, PISA3D has been applied to carefully model the welded moment connections, BRBs and EBFs in order to investigate the seismic performance of the 34-story steel structure under severe earthquakes.

DOI: 10.1002/eqe

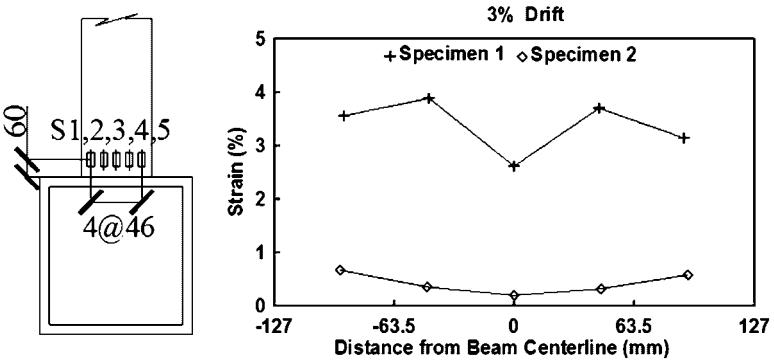

Figure 6. The location of strain gauges and tensile strain profiles.

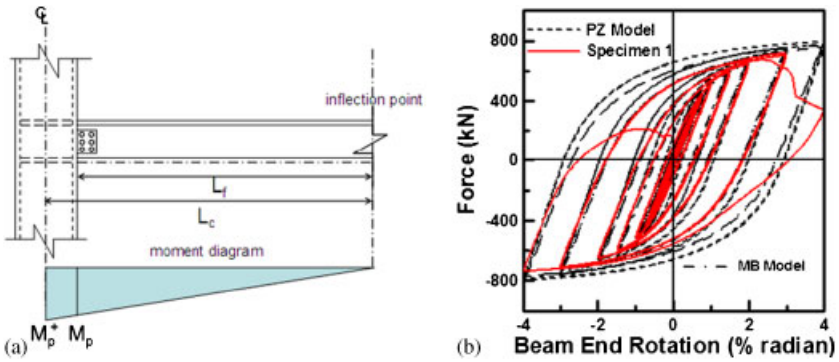

Figure 7. (a) Illustration of the moment gradient for flexural capacity modification and (b) hysteretic responses of the Specimen 1 obtained from experimental and analytical results using MB model and PZ model.

4.2. *Simplified analytical approach*

4.2.1. Welded beam-to-column moment connections. Without using the rigid end offset feature, the beam–column element flexural stiffness was computed from the node-to-node dimensions. The output of the force responses was also located at the nodal point. To simplify the analytical models and avoid the use of rigid end zones, the yield strength of the beam was modified so that yielding of the beam at the column face can be well represented. As shown in Figure 7(a), the beam plastic moment capacity was modified using the following equation

$$M_p^+ = M_p \cdot L_c / L_f \tag{1}$$

where M_p is the plastic moment capacity of the bare steel beam, M_p^+ is the modified beam moment capacity, L_c is the distance from the beam mid-span to the center of the column and L_f is the distance from the beam mid-span to the column face. Figure 7(b) shows the use of the plastic

DOI: 10.1002/eqe

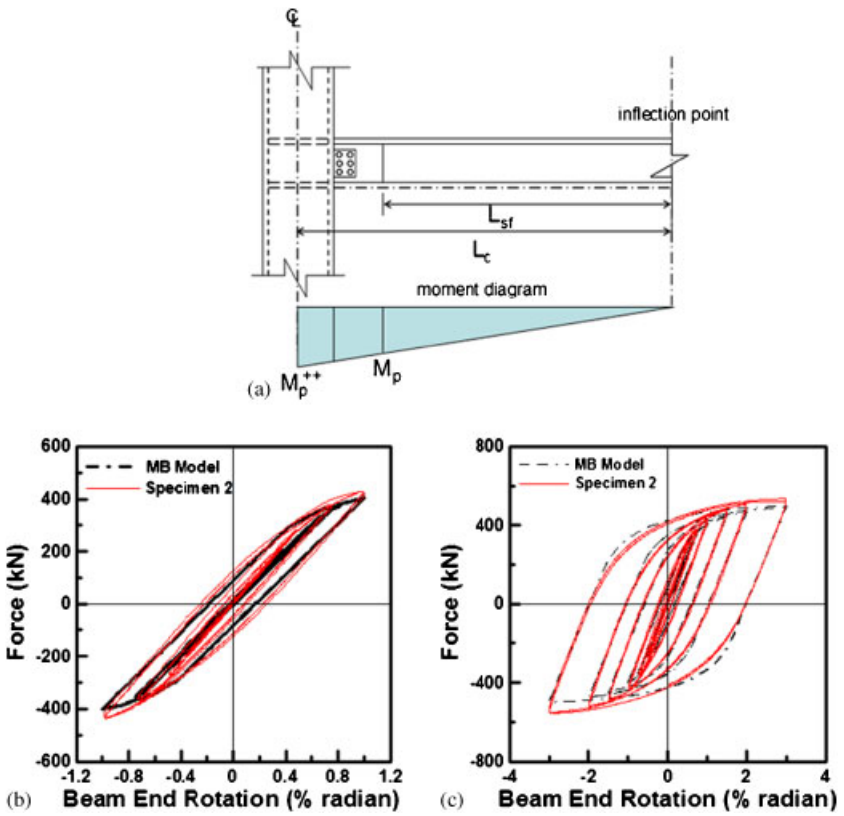

Figure 8. (a) Simplified moment capacity for MB model after strengthening; (b, c) hysteretic responses of the Specimen 2 obtained from experimental and analytical results using the MB model.

hardening material model and the proposed modification of the beam flexural capacity (modified beam, or MB Model) in simulating the experimental response of Specimen 1. The plastic hardening material model considers both isotropic and kinematic hardening commonly found in structural steel material. Figure 7(b) displays the simulation results derived from using the same material properties without modifying the beam flexural capacity but adopting the rigid end zone and a panel zone element (PZ model). It was found that both models simulated the test results quite well. However, the PZ model increases one degree of freedom at every beam-to-column moment connection. The same technique was found to be equally effective in modeling the stiffened welded moment connection for Specimen 2. The stiffened beam section was not built in the model. However, the plastic hinge was to be formed outside of the stiffeners. As shown in Figure 8(a), the beam plastic moment capacity was thus modified accordingly

$$M_p^{++} = M_p \cdot L_c / L_{sf} \tag{2}$$

where M_p^{++} is the modified plastic moment, and L_{sf} is the distance from the beam mid-span to the edge of the stiffeners. Figure 8(b) suggests that the proposed MB model can satisfactorily

DOI: 10.1002/eqe

simulate the experimental response at low-level deformations, whereas Figure 8(c) shows that the same MB model can accurately simulate the responses of Specimen 2 at large deformations. Thus, the MB model was adopted for all the welded moment connections in the 3-D structural model for the 34-story steel superstructure.

4.2.2. EBF shear-link beams. The beam element in PISA3D is able to simulate the shear and/or flexural yielding of the steel wide flange sections. Using the rigid end offset feature for link beam in EBF, the determination of shear yielding or flexural yielding is based on the clear length of the link beam. Therefore, the rigid end offset option was applied so that the shear and flexural strength of the link beam can be correctly incorporated into the determination of shear or flexural yielding. To simplify the analytical model, the PZ element was not considered at the link beam-to-column joint.

4.2.3. Buckling restrained braces. The proposed double-core BRB consists of the energy dissipation core yielding segment, the transition region and the core projection [9, 10]. The equivalent axial stiffness, K_e was computed for constructing the PISA3D model using the following equation:

$$K_e = \frac{E \cdot A_j \cdot A_t \cdot A_c}{2A_t \cdot A_c \cdot L_j + 2A_j \cdot A_c \cdot L_t + A_j \cdot A_t \cdot L_c} \tag{3}$$

where A_c, A_t, A_j and L_c, L_t, L_j are the cross-sectional area and the length of the energy dissipation core yielding segment, the transition region and the core projection, respectively. To examine the quality of the BRBs made by the fabricator, a BRB was arbitrary chosen and tested before the installation of all BRBs. The loading protocol and force versus deformation relationships for this A572 Gr.50 steel BRB specimens are shown with the actual yield capacity ($P_y = A_c \times F_{y,\text{actual}}$) in Figure 9. The BRB sustained the standard loading protocol [7] before the 19 cycles of constant strain (1.5 times the maximum considered earthquake induced strain, or $1.50 \times$ MCE strain) cyclic loading was applied. It was evident that the inelastic axial strain of the BRB specimen reached 0.022 (2 times of that associated with the design-story drift). From Figures 9(b) and (c), it can be found that the BRB specimen achieved a cumulative plastic deformation of 555 greater than the requirement (200 times the yield deformation) before fracture. Figure 9(d) shows the added BRB members installed at the construction site.

All BRB members were modeled using plastic hardening truss elements. In Figure 9(b), it is demonstrated that the PISA3D analytical model can accurately simulate the cyclic response of the BRB specimen. The vibration periods of the 1st to 6th mode of the original and the redesigned structures computed by PISA3D are listed in Table II, respectively.

5. SEISMIC RESPONSE ANALYSIS USING SYNTHETIC GROUND MOTIONS

5.1. Ground motions

The phase angles of three historical ground motion records: KAUEW, KAUNS and KAUPNS, were selected for the construction of the synthetic ground accelerations (Figure 10(a)). These three records (Table III) were recorded in Kaohsiung during a recent earthquake that struck at the southern coast of Taiwan on December 26th in 2006 [11]. Figure 10(b) shows the three synthetic ground accelerations, denoted as AKAUEW (EQ1), AKAUNS (EQ2) and AKAUPNS (EQ3). Figure 10(c)

DOI: 10.1002/eqe

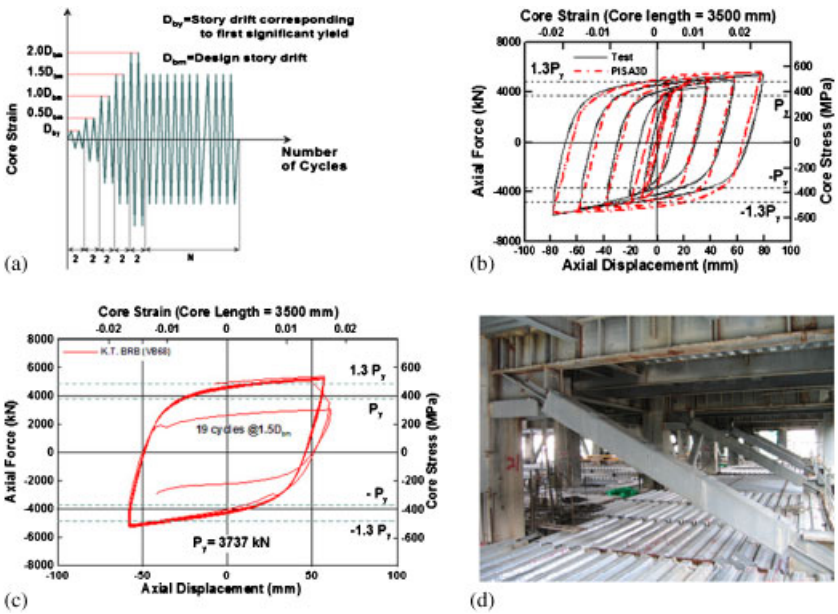

Figure 9. (a) BRB loading protocol; (b) hysteretic responses of the BRB specimen; (c) low cycle fatigue test; and (d) a photo of BRB members at the construction site.

Table II. 1st to 6th modal periods of the original structure and the redesigned structure.

	Original (unit: second)	Redesigned (unit: second)
1st Mode	$T_{1,O}=4.27$	$T_{1,R}=3.75$
2nd Mode	3.88	3.59
3rd Mode	3.74	3.21
4th Mode	1.80	1.21
5th Mode	1.57	1.18
6th Mode	1.44	1.08

confirms that the response spectra of the three synthetic ground motions are compatible with the elastic design spectrum suggested by Code '05 for a MCE-level (PGA $=0.32g$) earthquake.

5.2. Seismic performance evaluation

5.2.1. Nonlinear response history analysis (NLRHA) and incremental dynamic analysis (IDA). The NLRHA was conducted for both the DE-level (PGA $=0.29g$) and the MCE-level (PGA $=0.32g$) earthquakes. However, it was found that the responses of the superstructure were similar under the excitation of these two levels of earthquake. Only the key responses of the original and the redesigned structures under the MCE-level earthquakes are presented. The peak-story displacements, peak inter-story drifts and the peak-story shears under the application of these three synthetic earthquakes of MCE-level are shown in Figures 11(a), (b) and (c), respectively.

DOI: 10.1002/eqe

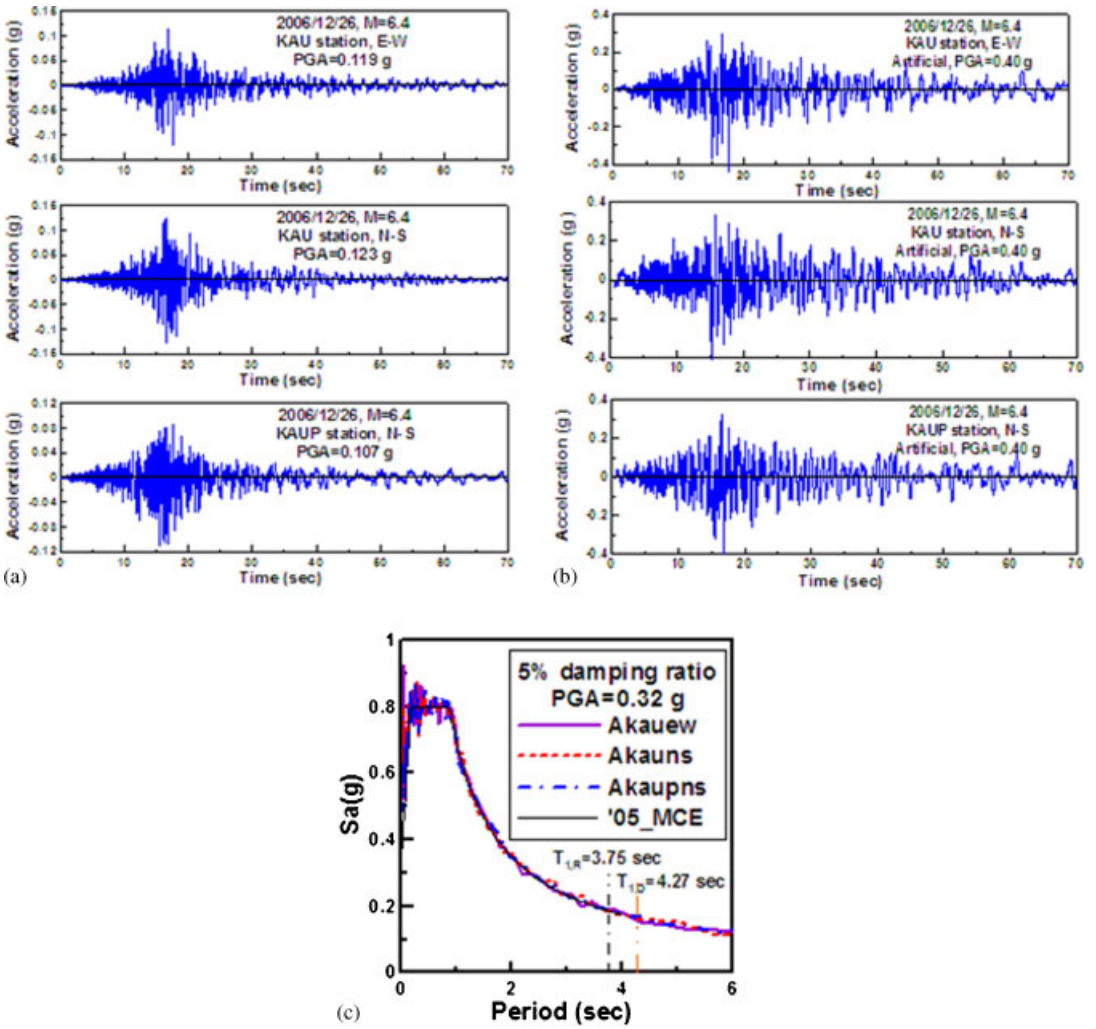

Figure 10. (a) Original historical ground motion records; (b) synthetic ground accelerations; and (c) the design compatible elastic spectra.

Figure 11(a) shows peak roof displacement reached 1.12 and 1.03 m for the original and redesigned structures, respectively. Figure 11(b) shows peak inter-story drifts are reduced from the 1st to 11th floors, but increased from the 26th to 34th floors after retrofitting. This could be because the floor weight in some lower floors was reduced while that of the higher floors were increased. Peak inter-story drifts of the original and the redesigned structures reached 0.012 and 0.014 rad, respectively.

Nevertheless, the peak inter-story drift demand (0.014 rad) under the MCE-level excitation was still small enough to meet the life-safety performance criterion (0.015 rad) for new steel braced frames suggested in FEMA-450 [12]. Figure 11(c) shows that almost all the peak-story shears were increased slightly after the structure was retrofitted. IDA [13] was conducted using the same

DOI: 10.1002/eqe

Table III. Earthquake records used in this study.

Records, Component	Epicenter distance (km)	PGA (g)
KAU, EW	26.7	0.119
KAU, NS	26.7	0.123
KAUP, NS	27.3	0.107
SPT, EW	29.6	0.088
SPT, NS	29.6	0.093
SGL, EW	35.1	0.073
SGL, NS	35.1	0.083

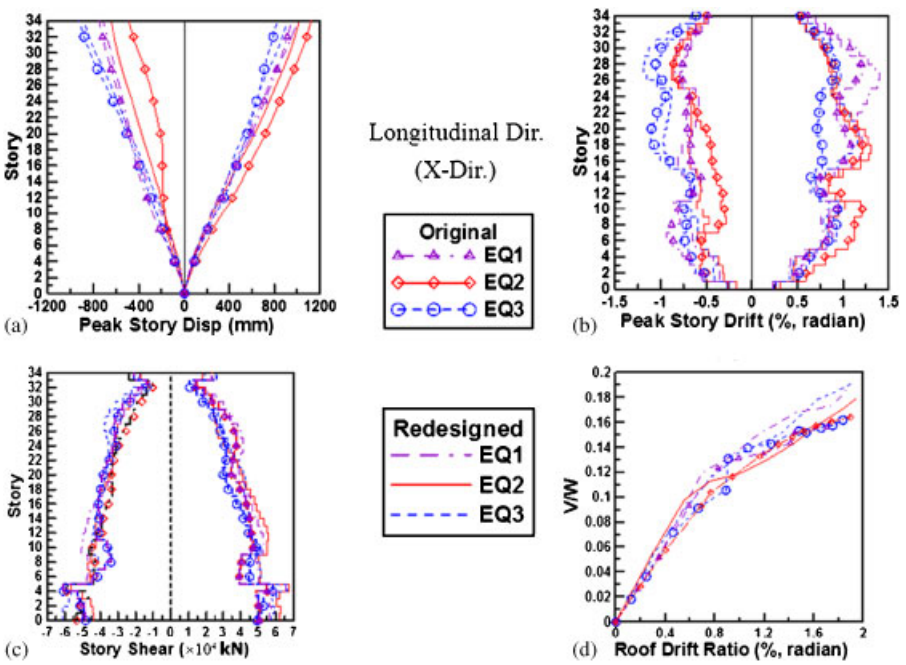

Figure 11. Comparison of longitudinal peak seismic responses between the original and redesigned structures induced by synthetic ground motion records: (a) peak-story displacement; (b) peak inter-story drift; (c) peak-story shear; and (d) the capacity curves of the redesigned structure obtained from IDA.

three earthquakes to compare the capacities between the original and the redesigned structures. The resulting roof drift versus the base shear to building weight ratio relationships are shown in Figure 11(d). It can be found that the lateral stiffness and the strength of the original structure are smaller than those of the redesigned. Although the dynamic responses of the original structure were not significantly reduced after retrofitting, the owner and the design engineer of the building decided to add response modification elements into the reconstruction. It is because that the pre-Northridge type of welded moment connection adopted in the original structure may not be able to reliably provide sufficient deformational capacities, especially when the original structural frame was exposed to weathering for more than 10 years.

DOI: 10.1002/eqe

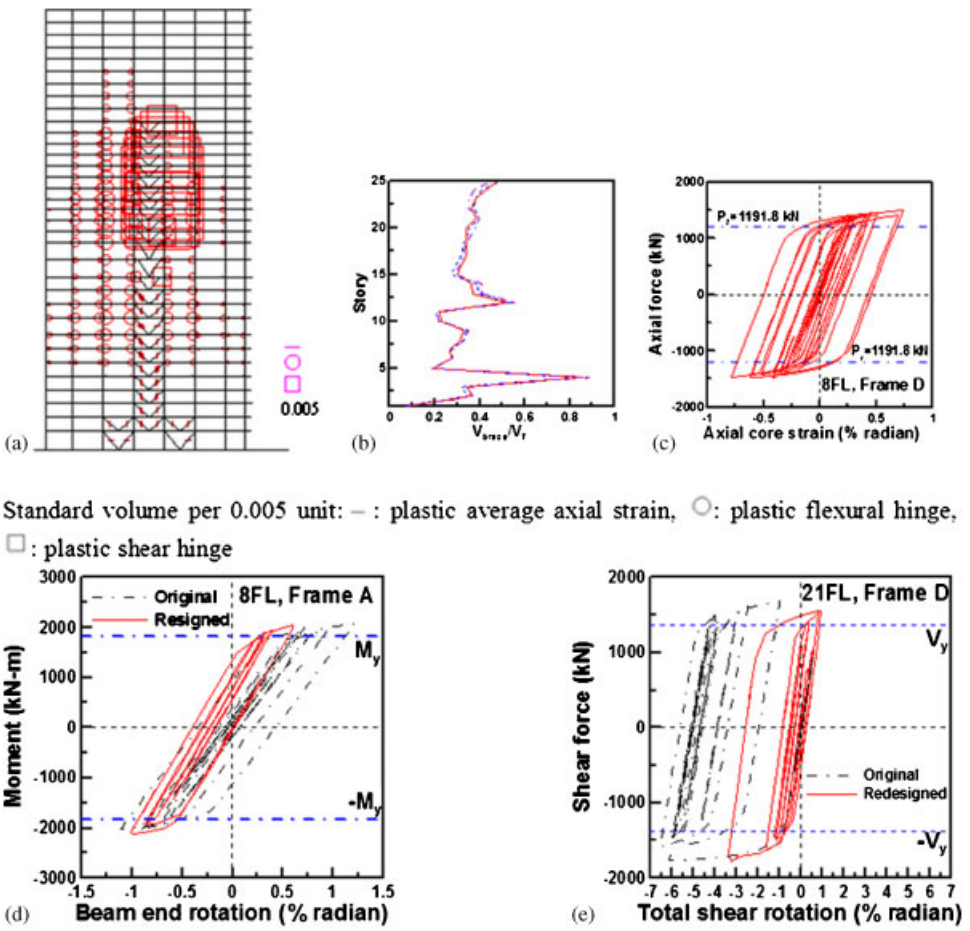

Figure 12. Nonlinear seismic responses: (a) plastic hinge distribution in Frame D of the redesigned building; (b) peak $V_{\text{brace}}/V_{\text{T}}$ ratio of the redesigned building; (c) BRB member; (d) welded moment connection; and (e) shear-link beam induced by the EQ3 acceleration record for the MCE-Level (PGA = 0.32g).

Under the MCE-level EQ3 earthquake applied in the longitudinal direction, Figure 12(a) illustrates the plastic hinge distributions in frame line D of the redesigned structure. Figure 12(b) indicates that the ratios between the brace shear V_{braces} and story shear V_{T} along the building height range from 0.1 to 0.9. Figures 12(c), (d) and (e) show the corresponding hysteretic responses of some specific structural members where nonlinear responses are more pronounced than elsewhere: BRB member at 8th floor, shear-link beam at 21st floor and welded moment connection at 8th floor, respectively. The stated BRB peak axial core strain demand was about 0.077 (Figure 12(c)), and the peak total beam end flexural rotation demand reached 0.01 rad (Figure 12(d)). Figure 12(e) shows that the link beam total shear rotation demands of the original and redesigned buildings reached 0.065 and 0.033 rad, respectively. Both are smaller than the 0.08 rad recommended for the shear link [7]. Clearly, some of the EBF link beam rotational demand in the original structure has been significantly reduced. The analyses also suggest that the rotational demand imposed on

DOI: 10.1002/eqe

the welded moment connection is only about 0.01 rad, much smaller than the rotational capacity (0.04 rad) found in the test results of the retrofitted connection.

6. SCALING OF HISTORICAL GROUND MOTIONS

As shown above, synthetic ground motions have been applied in the response analyses of the example building. Generally speaking, spectrum compatible method may be more appropriate where fewer ground motions are used. However, effects of spectrum matching on nonlinear response are not well understood at this time. Some engineers are concerned with skewing the energy content of ground motions through spectrum matching, which may have an unknown effect on the nonlinear response. To gain insights into the nonlinear responses of the example structure under the excitation of historical ground accelerations, further NLRHA were conducted. The techniques of ground motion scaling methods [2, 14, 15] have also been studied in this research. Two of the most common ground motion scaling methods used in Taiwan are as follows:

1. Code method: the ground motion scaling procedure prescribed in Code'05 [1]. Given a suite of ground motion records, a scale factor is applied to each record to either increase or decrease its intensity. If T_1 is the fundamental vibration period of the building in the considered direction, each scale factor is selected such that the corresponding spectral accelerations between the period range from 0.2 T_1 to 1.5 T_1 satisfy the following two requirements: (1) Any spectral acceleration of the given ground motion shall be greater than 0.9 times that of the design response spectrum; and (2) The average of response spectrum from the scaled motion does not fall below the target design response spectrum.
2. $Sa(T_1)$ method [2]: each ground motion is scaled so that its spectral acceleration value, $Sa(T_1)$, at the linear-elastic fundamental period of the structure being analyzed, matches the design spectrum.

Both the Code and $Sa(T_1)$ methods depend on the structural dynamic characteristic (T_1) as well as the frequency contents of the ground motion. Currently, there is no consensus on the preferable approach (scaling or spectrum compatible) for nonlinear dynamic analysis. The advantage of scaling method is that individual ground motion record retains its original characteristics including peaks and valleys in the response spectrum. However, to avoid the response being uncharacteristically dominated by the peaks and valleys of any one ground motion, it is recommended that no less than seven ground motion records are to be used [14]. In addition, when the scaling approach is adopted, the upper limit of the scale factor should be 4 and 6 for 10/50 and 2/50 yr hazard levels, respectively [16]. Nevertheless, for high-rise buildings, high-mode effects can be rather pronounced. If a ground acceleration record is scaled without properly incorporating the design spectral acceleration values at the significant periods of a building, it can seriously overestimate or underestimate the seismic demands. This argument will be verified later in this paper. To properly incorporate the high-mode effects in the estimation of the seismic demand, the MMS methods were investigated and presented in this paper.

6.1. Multi-mode ground motion scaling procedure

The general idea of MMS is to minimize the modal participating difference between the spectral accelerations or displacements of a scaled ground motion and that of the smoothed design response spectra for the first few modes. According to the response spectra analysis (RSA) procedure [17],

DOI: 10.1002/eqe

the peak modal responses can be estimated by adopting the square-root-of-sum-of-squares (SRSS) or the complete quadratic combination rules. For discussion purposes, the SRSS rule is used to illustrate the computation of the scaling factor for the MMS method. If r_{n0} is the peak value of the nth mode contribution $r_n(t)$ to the total response $r(t)$, then the peak total response r_0 is:

$$r_0 \approx \left(\sum_{n=1}^{N} r_{n0}^2 \right)^{1/2} \tag{4}$$

The base shears (V_{d} and V_{EQ}), and roof displacements ($u_{\mathrm{roof,d}}$ and $u_{\mathrm{roof,EQ}}$) can be expressed as

$$V_{\mathrm{d}} = \sqrt{\sum_{n=1}^{N} (\Gamma_i L_i S_{ai,\mathrm{des}})^2}, \quad V_{\mathrm{EQ}} = \sqrt{\sum_{n=1}^{N} (\Gamma_i L_i S_{ai,\mathrm{EQ}})^2} \tag{5}$$

and

$$u_{\mathrm{roof,d}} = \sqrt{\sum_{n=1}^{N} (\Gamma_i S_{ai,\mathrm{des}}/\omega_i^2)^2}, \quad u_{\mathrm{roof,EQ}} = \sqrt{\sum_{n=1}^{N} (\Gamma_i S_{ai,\mathrm{EQ}}/\omega_i^2)^2} \tag{6}$$

where V_{d} (or $u_{\mathrm{roof,d}}$) and V_{EQ} (or $u_{\mathrm{roof,EQ}}$) are calculated from the smoothed design spectrum and the spectrum obtained from the natural earthquake accelerations, respectively. On the other hand, ω_i is the ith vibration frequency of the MDF system; Γ_i and L_i are the modal participation factor and modal excitation factor of the ith mode, respectively; finally, $S_{ai,\mathrm{des}}$ and $S_{ai,\mathrm{EQ}}$ are the spectral accelerations in the smoothed design spectrum and the spectrum obtained from the natural earthquake accelerations, respectively.

6.2. Computation of the scaling factors from the MMS method

The least-square error fitting method was used to reduce the modal participating difference between the first few modal spectral accelerations or displacements of a scaled ground motion and that of the smoothed design response spectra. For example, the desired number of the first few modes N is three. The corresponding smoothed spectral accelerations are $S_{a1,\mathrm{des}}$, $S_{a2,\mathrm{des}}$ and $S_{a3,\mathrm{des}}$, and those of the original unscaled spectral accelerations are $S_{a1,\mathrm{EQ}}$, $S_{a2,\mathrm{EQ}}$ and $S_{a3,\mathrm{EQ}}$, respectively. Therefore, the square error of these two sets of accelerations can be expressed as

$$\begin{aligned} (\mathrm{error})^2 = {} & W_1[S_{a1,\mathrm{des}} - \mathrm{SF}\cdot S_{a1,\mathrm{EQ}}]^2 + W_2[S_{a2,\mathrm{des}} - \mathrm{SF}\cdot S_{a2,\mathrm{EQ}}]^2 \\ & + W_3[S_{a2,\mathrm{des}} - \mathrm{SF}\cdot S_{a3,\mathrm{EQ}}]^2 \end{aligned} \tag{7}$$

where SF is the scaling factor, whereas W_1, W_2 and W_3 are the weighting factors associated with the first three modes, respectively. The minimum error can then be achieved when the partial derivative of error^2 with respect to the SF becomes zero:

$$\frac{\partial(\mathrm{error}^2)}{\partial(\mathrm{SF})} = 0 \tag{8}$$

Hence, the SF can be expressed as:

$$\mathrm{SF} = \frac{W_1 \cdot S_{a1,\mathrm{des}} \cdot S_{a1,\mathrm{EQ}} + W_2 \cdot S_{a2,\mathrm{des}} \cdot S_{a2,\mathrm{EQ}} + W_3 \cdot S_{a2,\mathrm{des}} \cdot S_{a2,\mathrm{EQ}}}{W_1 \cdot (S_{a1,\mathrm{EQ}})^2 + W_2 \cdot (S_{a2,\mathrm{EQ}})^2 + W_3 \cdot (S_{a3,\mathrm{EQ}})^2} \tag{9}$$

DOI: 10.1002/eqe

Since the elastic peak base shear V_i and roof displacement $u_{\text{roof},i}$ of ith mode are expressed as $\Gamma_i L_i S_{ai}$ and $\Gamma_i \phi_i S_{ai}/\omega_i^2$, respectively (refer to Equations (5) and (6)), it is proposed that the weighting factors W_i for each mode be expressed as shown below for the computation of scaling factors. For computation of base shear

$$W_i = \frac{\Gamma_i^2 L_i^2}{\sum_{i=1}^{N} \Gamma_i^2 L_l^2} \quad (i = 1 \sim N) \tag{10a}$$

whereas for computation of roof displacement

$$W_i = \frac{(\Gamma_i/\omega_i^2)^2}{\sum_{i=1}^{N} (\Gamma_i/\omega_i^2)^2} \quad (i = 1 \sim N) \tag{10b}$$

Thus, weighting factors given in Equation (10a) can be applied in Equation (9) for the computation of scaling factors when base shear is considered as the key design parameter, whereas Equation (10b) can be applied when the roof displacement is the key parameter of interest. These two weighting factors (Equations (10a) and (10b)) and the corresponding ground motion scaling factors will be applied in order to examine their effectiveness in the seismic performance evaluations of the retrofitted 34-story example building. Since the proposed method incorporates multiple modes into the scaling (MMS) procedures, for the purpose of discussion, the method is identified as MMS-V (V for shear) or MMS-D (D for displacement) when Equation (10a) or Equation (10b) is applied, respectively. It is important to consider the recommendation that the number of modes to be determined includes at least 90% of the total building mass when the RSA method is applied [14]. Lopez and Cruz [18] have also proposed some empirical formulas to determine the minimum number of modes N for the response computations. For the purpose of illustrating the effectiveness of the MMS method, only three modes (constitute 84% of the total building mass) were incorporated into the computation of the scaling factors and the response spectra shown in Figure 13(a). Table IV shows the modal participation factors Γ_i, modal excitation factors L_i, spectral accelerations $S_{ai,\text{des}}$ computed from the smoothed MCE spectrum and each scaled historical earthquake for the first three modes in the x-direction. In Table IV, the first three modal spectral accelerations in the response spectra computed from the aforementioned seven unscaled historical earthquakes are also provided.

6.3. Comparing the MMS with the Code and $S_a(T_1)$ methods

Seven natural ground motion records listed in Table III were used to investigate the variability of seismic demands computed using different ground motion scaling methods. For the 34-story steel building, the first three vibration periods are 3.75 s (T_{1x}), 1.21 s (T_{2x}) and 0.68 s (T_{3x}) in the longitudinal direction. Figure 13(a) shows the smoothed 5% damped elastic acceleration response spectrum of the MCE. In the same figure, four other response spectra (constructed from the averaged responses of the seven historical earthquakes scaled according to four different rules) are also compared. They include the Code, $S_a(T_1)$, MMS-V and MMS-D methods described previously. Figure 13(b) shows the COVs, with respect to the smoothed MCE response spectrum, computed from the four scaling methods. It is evident in Figure 13(a) that the average of seven spectra computed using MMS-V method is closer to the smoothed design spectrum in the range from T_{3x} to T_{1x}. Figure 13(b), on the other hand, shows a significant reduction in the scatter of the spectral acceleration computed using MMS-V method for vibration periods less than about

DOI: 10.1002/eqe

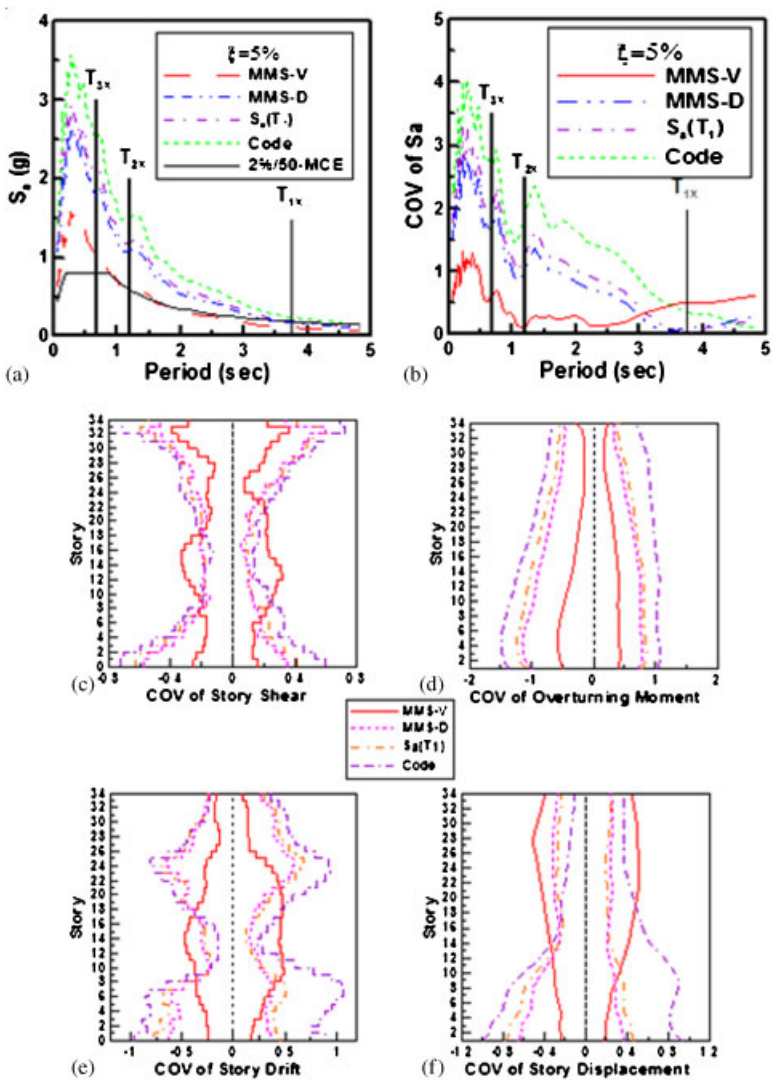

Figure 13. (a) The mean elastic 5-damped spectral acceleration; (b) the corresponding COV spectrum and scatter in MDOF seismic demands after seven ground motion records scaled by four scaling methods; the COVs of the peak seismic demands along the building height: (c) story shear; (d) overturning moment; (e) story drift; and (f) story displacement.

3.0 s This study therefore is able to compare the effectiveness of the MMS-V and MMS-D to the Code or $S_a(T_1)$ methods in reducing the scatter of the peak seismic demands computed from both the RSA and NLRHA.

6.3.1. Response Spectral Analysis (RSA). Assuming the structural system remains elastic under the effects of all magnitude of earthquakes, $V_d = 91958$ kN and $u_{roof,d} = 991.7$ mm can be computed

DOI: 10.1002/eqe

Table IV. Modal parameters and spectral accelerations computed from the smoothed MCE-level spectrum and unscaled historical records.

Mode	ω_i (cps)	Γ_i	L_i	$S_{ai,\mathrm{des}}$	Original spectral acceleration $S_{ai,\mathrm{EQ}}$ (g)						
					KAU, EW	KAu, NS	KAUP, NS	SGL, EW	SGL, NS	SPT, EW	SPT, NS
1st	1.68	1.49	20441	0.19	0.02	0.02	0.03	0.02	0.02	0.01	0.02
2nd	5.20	−0.93	−13398	0.58	0.11	0.14	0.11	0.13	0.10	0.07	0.14
3rd	9.30	0.30	7735	0.8	0.12	0.16	0.15	0.18	0.29	0.19	0.17

Table V. Comparison of elastic seismic responses using four different ground motion scaling methods.

Methods	EQ records	W_1	W_2	W_3	SF	PGA (g)	V_{EQ} (kN)	$u_{\mathrm{roof,EQ}}$ (mm)	$V_{\mathrm{EQ}}/V_{\mathrm{d}}$	$u_{\mathrm{roof,EQ}}/u_{\mathrm{roof,d}}$
MMS-V	KAU, EW	0.854	0.141	0.005	5.97	0.72	87437	568.6	0.95	0.57
	KAU, NS				4.76	0.56	88575	532.5	0.96	0.54
	KAUP, NS				5.58	0.61	91838	927.8	0.98	0.94
	SGL, EW				5.07	0.36	86554	509.4	0.94	0.51
	SGL, NS				5.81	0.47	87007	627.1	0.95	0.63
	SPT, EW				8.24	0.71	88784	470.9	0.97	0.47
	SPT, NS				4.65	0.42	87017	524.7	0.95	0.53
MMS-D	KAU, EW	0.996	0.004	0.000	10.2	1.23	149070	969.3	1.62	0.98
	KAU, NS				8.66	1.02	161222	969.2	1.75	0.98
	KAUP, NS				5.97	0.65	98136	991.4	1.07	1.00
	SGL, EW				9.57	0.68	163200	960.4	1.77	0.97
	SGL, NS				9.10	0.74	136230	981.9	1.48	0.99
	SPT, EW				17.0	1.47	182916	970.2	1.99	0.98
	SPT, NS				8.55	0.78	159823	963.6	1.74	0.97
$S_a(T_1)$	KAU, EW	N.A.	N.A.	N.A.	11.1	1.34	162282	1055	1.76	1.06
	KAU, NS	N.A.	N.A.	N.A.	9.63	1.14	179288	1078	1.95	1.09
	KAUP, NS	N.A.	N.A.	N.A.	6.00	0.65	98623	996.4	1.00	1.00
	SGL, EW	N.A.	N.A.	N.A.	10.8	0.77	183543	1080	1.99	1.09
	SGL, NS	N.A.	N.A.	N.A.	9.51	0.78	142377	1026	1.55	1.03
	SPT, EW	N.A.	N.A.	N.A.	19.3	1.66	207408	1100	2.26	1.11
	SPT, NS	N.A.	N.A.	N.A.	9.53	0.87	178285	1075	1.94	1.08
Code	KAU, EW	N.A.	N.A.	N.A.	10.4	1.26	152768	993.4	1.66	1.00
	KAU, NS	N.A.	N.A.	N.A.	11.6	1.37	216691	1303	2.36	1.31
	KAUP, NS	N.A.	N.A.	N.A.	7.29	0.79	119946	1212	1.3	1.22
	SGL, EW	N.A.	N.A.	N.A.	14.9	1.06	253632	1493	2.76	1.51
	SGL, NS	N.A.	N.A.	N.A.	13.8	1.12	206575	1489	2.25	1.50
	SPT, EW	N.A.	N.A.	N.A.	20.85	1.80	224559	1191	2.44	1.20
	SPT, NS	N.A.	N.A.	N.A.	15.0	1.36	280464	1691	3.05	1.71

from Equations (5) and (6), respectively. Table V displays the weighting factors, W_i computed using Equations (10a) and (10b). The scaling factors SF and the corresponding PGA values, base shears V_{EQ} and V_{d}, roof displacements $u_{\mathrm{roof,EQ}}$ computed from Equations (5) and (6) are also provided. In addition, the $V_{\mathrm{EQ}}/V_{\mathrm{d}}$ and $u_{\mathrm{roof,EQ}}/u_{\mathrm{roof,d}}$ ratios were calculated. When the ratio is closer to 1.0, this implies that the estimate of the peak seismic shear or roof displacement demand

DOI: 10.1002/eqe

is closer to that computed from the smoothed response spectrum. Clearly, with the exception of the MMS-V method, the scaling factors determined from the MMS-D, $Sa(T_1)$ and Code methods have all exceeded the suggested limit of 6.0. For each earthquake, the MMS-V method evidently provides the best agreement between V_{EQ} and V_d. In addition, as indicated in Table V, the MMS-D method provides the best estimate of the peak roof displacement compared with the other three methods.

6.3.2. Nonlinear response history analyses (NLRHA). NLRHA were conducted by applying the scaling factors shown in Table V for the seven ground motions. In addition, arithmetic mean of the peak values obtained via NLRHA using the three MCE-level synthetic ground motions was first computed, subsequently the COV of the specific peak responses computed for the seven ground motions can be ascertained. The COVs are presented for four key responses along the height of the superstructure.

6.3.3. Variability of peak-story shear. Figure 13(c) shows the COVs of the peak-story shear profiles along the building height in the longitudinal direction using the four described methods. The results suggest that the MMS-V method significantly reduces the variation of the peak-story shear demand estimate from the ground floor to the 6th floor and from the 25th floor to the 34th floor compared with other scaling methods.

6.3.4. Variability of peak overturning moment. On the other hand, Figure 13(d) shows the COVs of the peak overturning moment profiles in the longitudinal direction. The results indicate that the MMS-V method provides an effective reduction of the scatter in the peak overturning moment along the full building height compared with the other three scaling methods.

6.3.5. Variability of peak inter-story drift. Next, Figure 13(e) shows similar trends for the COVs of the peak inter-story drift profiles. The COVs computed for the MMS-D, $Sa(T_1)$ and Code methods vary noticeably along the building height, but its magnitude and variation are significantly reduced when using the MMS-V method.

6.3.6. Variability of peak-story displacement. Lastly, Figure 13(f) shows the COV values of the peak-story displacement profiles along the building height. It can be deduced that the MMS-D and $Sa(T_1)$ methods fare better in reducing the scatter of the story displacement for upper floors compared with other scaling methods. The effectiveness of the MMS-D method in reducing the scatter of the peak-story displacement along the building height is hence demonstrated.

7. CONCLUSIONS

From the experimental and analytical studies, the following conclusions can be drawn:

(a) The proposed beam-to-column connection stiffening scheme using two steel web side plates can be conveniently installed in the welded moment connections without removing the existing concrete slab above the beam flange;
(b) Test confirms that the proposed side-plate stiffening scheme is effective in preventing the fracture occurred in the beam flange. The stiffened welded moment connection possesses a

DOI: 10.1002/eqe

larger rotational capacity than that in the original pre-Northridge type connection. A separate study [19] has also confirmed its effectiveness and the design method using cyclic tests and finite element analysis for nine additional specimens;

(c) The proposed analytical models are found to be accurate in simulating the experimental responses of BRB member, and welded moment connections before and after stiffening;

(d) Nonlinear dynamic analyses confirmed that the rotational demand on the EBF link beams has been significantly reduced by adopting the response modification elements in the redesigned structure;

(e) NRHA show that almost all the story shear demands were increased slightly after the structure was retrofitted. Analytical results indicate that the ratios between the brace shear and story shear along the building height range from 0.1 to 0.9;

(f) With the exception of the MMS-V method, the scaling factors determined from the MMS-D, $S_a(T_1)$ and Code methods exceeded the suggested limit. Furthermore, it appears that the other three methods often lead to overestimation of the seismic force responses for the building. The proposed MMS-D method provides the best estimate of the peak roof displacements among all the methods adopted; and

(g) The MMS-V method provides an effective reduction in the scatter of the estimates of the peak-story shear, overturning moment and peak inter-story drift. Owing to its simplicity and inclusion of multi-mode effects, the MMS-V method is deemed to be more applicable for the example building than the other scaling methods considered in this study.

REFERENCES

1. ABRI *Recommended Provisions for Building Seismic Regulations*. ABRI, Taipei, 2005 (in Chinese).
2. Shome N, Cornell C. Normalization and scaling accelerograms for nonlinear structural analysis. *Sixth U.S. National Conference on Earthquake Engineering*, Seattle, WA, 1998 (CD-ROM).
3. Vidic T, Fajfar P, Fischinger M. Consistent inelastic design spectra: strength and displacement. *Earthquake Engineering and Structural Dynamics* 1994; **23**:507–521.
4. Miranda E. Site-dependent strength-reduction factors. *Journal of Structural Engineering* (ASCE) 1993; **119**: 3503–3519.
5. Nau J, Hall W. Scaling methods for earthquake response spectra. *Journal of Structural Engineering* (ASCE) 1984; **110**:91–109.
6. ABRI *Recommended Provisions for Building Seismic Regulations*. ABRI, Taipei, 1989 (in Chinese).
7. AISC *Seismic Provisions for Structural Steel Buildings*. AISC, Chicago, IL, 2005.
8. Lin BZ, Chuang MC, Tsai KC. Object-oriented development and application of a nonlinear structural analysis framework. *Advances in Engineering Software* 2008; **40**:66–82. DOI: 10.1016/j.advengsoft.2008.03.012.
9. Tsai KC, Hsiao PC, Weng YT, Lin ML, Lin KC, Chen CH, Lai JW, Lin SL. Pseudo-dynamic tests of a full-scale CFT/BRB frame. Part 1: specimen design, experiment and analysis. *Earthquake Engineering and Structural Dynamics* 2008; **37**:1081–1098.
10. Tsai KC, Hsiao PC. Pseudo-dynamic tests of a full-scale CFT/BRB frame. Part 2: seismic performance of buckling restrained braces and connections. *Earthquake Engineering and Structural Dynamics* 2008; **37**:1099–1115.
11. NCDR and NCREE. *The Preliminary Reconnaissance Report of 2006 Hengtsun Earthquake*. NCDR and NCREE, December 2006 (in Chinese).
12. BSSC. *NEHRP Recommended Provisions for Seismic Regulations for New Buildings and Other Structures*. Federal Emergency Management Agency: Washington, DC, 2003.
13. Vamvatsikos D, Cornell CA. Incremental dynamic analysis. *Earthquake Engineering and Structural Dynamics* 2002; **31**(3):491–514.
14. International Council of Building Officials (ICBO). *Uniform Building Code*. International Council of Building Officials (ICBO), Whittier, CA, 2006.
15. Kurama YC, Farrow KT. Ground motion scaling methods for different site conditions and structure characteristics. *Earthquake Engineering and Structural Dynamics* 2003; **32**:2425–2450.

16. Malhotra PK. Strong-motion records for site-specific analysis. *Earthquake Spectra* 2003; **19**(3):557–578.
17. Chopra AK. *Dynamic of Structures*: *Theory and Applications to Earthquake Engineering* (2nd edn). Prentice-Hall: Englewood Cliffs, NJ, 2003.
18. Lopez OA, Cruz M. Number of modes for the seismic design of buildings. *Earthquake Engineering and Structural Dynamics* 1996; **25**:837–855.
19. Chou CC, Tsai KC, Wang YY, Jao CK. Seismic performance of steel site plate moment connections. *14th World Conference on Earthquake Engineering*, Beijing, 2008; 12–17.

DOI: 10.1002/eqe